Journal of the Serbian Chemical Society
JSCS-info@shd.org.rs • www.shd.org.rs/JSCS

ACCEPTED MANUSCRIPT

Journal of the Serbian Chemical Society
JSCS-info@shd.org.rs • www.shd.org.rs/JSCS
J. Serb. Chem. Soc. **00(0)** 1-14 (2022)
JSCS–12081
Original scientific paper
Published DD MM, YYY

Curcumin as a potential multiple-target inhibitor against SARS-CoV-2 Infection: A detailed interaction study using quantum chemical calculations

SUMIT KUMAR *

Department of Chemistry, Magadh University, Bodh Gaya-824234, Bihar, India

(Received 21 September, Revised 21 November; Accepted 28 December 2022)

Abstract: Curcumin is one of the important naturally occurring compounds having several medicinal properties such as antiviral, antioxidant, antifibrotic, antineoplastic as well as anti-inflammatory properties. SARS-CoV-2 has emerged as infectious virus, which severely infected a large group of population in the world. Several efforts have been made to prepare novel antiviral compound but it is challenging even after rigorous trials. Naturally occurring compound, curcumin, can be used as an alternative of antiviral compound against SARS-CoV-2. Its effect against SARS-CoV-2 is already highlighted in the literature. But the quantitative study of its interaction with various precursors of SARS-CoV-2 is not reported till date. This paper reports the interaction of curcumin with angiotensin-converting enzyme2, transmembrane serine protease 2, 3-chymotrypsin-like protease and papain-like protease through molecular docking and quantum chemistry calculations to achieve quantitative understanding of underlying interactions. Here the conformational flexibility of curcumin is also highlighted, which helps it to accommodate in the four different docking sites. The study has been performed using calculations of geometrical parameter, atomic charge, electron density, Laplacian of electron density, dipole moment and the energy gap between highest occupied and lowest unoccupied molecular orbitals. The non-covalent interaction (NCI) analysis is performed to visualize the weak interaction present in the active sites. Combinedly molecular docking and detailed quantum chemistry calculations revealed that curcumin can be adopted as a potential multiple-target inhibitors against SARS-CoV-2.

Keywords: antiviral drug, non-covalent interaction, charge density analysis, atom-in-molecule calculation, angiotensin-converting enzyme2, transmembrane serine protease 2

* Corresponding author E-mail: sumitkrmgr@gmail.com
https://doi.org/10.2298/JSC220921087K

INTRODUCTION

In the last couple of years, coronavirus 2 (SARS-CoV-2) widely spread and affected over more than 600 million population of the world and 6.5 million people died according to world health organization (https://www.who.int/). Considering this situation world health organization already characterized it as pandemic in 2020. In comparison to middle east respiratory syndrome coronavirus (MERS-CoV), SARS-CoV-2 has been found more contagious and therefore infected fast a large group of population.[1] The development of novel antivirals against SARS-CoV-2 is always a matter of interest as well as a challenge in front of the scientific community. An enormous number of efforts are made to validate antiviral compounds. Some naturally occurring compounds already have antiviral properties, which can be used as an alternative to antiviral complex compounds evolved during the development of novel antivirals.[2-3] Curcumin, a yellow pigmented polyphenolic compound, is majorly found in turmeric used as a food additive.[4] Its antiviral activity against SARS-CoV-2 along with other viral infections are already reported in the literature.[5-9] It is an interesting natural occurring substance, which also has antioxidant, antifibrotic, antineoplastic as well as anti-inflammatory properties.[4, 10]

SARS-CoV-2 belongs to fusion protein containing two major subunits (S1 and S2).[11] For the spread of SARS-CoV-2, angiotensin-converting enzyme2 plays a major role to determine its entry through interaction with viral spike protein.[11-12] Further transmembrane serine protease 2 (TMPRSS2) cleaves the spike protein into smaller subunits, which leads to subsequent cellular entry of infectious viral RNA.[13-16] Upon entry to the cell, two SARS-CoV-2 proteases 3-chymotrypsin-like protease (3CLpro, also known as main protease, Mpro) and papain-like protease (PLpro) cleaves the proteins.[13-16] Both 3CLpro and PLpro are essential for the release of 16 non-structural proteins (nsps) on breaking down of polyprotein.[13-16] Further the replication and transcription occur to produce viral genomes by accumulation of infectious replicase on the host membrane.[17] Later the four major proteins the spike (S) protein, membrane (M) protein, nucleocapsid (N) protein, and the envelope (E) protein form and leads to the formation of viral particle. Some viral particle of CoVs is also reported without using full ensemble of all four proteins by encoding extra protein having similar or compensatory ability.[18-20] Till date there is no report available in the literature providing in-depth molecular level study of interaction of curcumin along with TMPRSS2, ACE2, PLpro and 3CLpro to understand its ability to encounter with SARS-CoV-2. Therefore, the study of curcumin along with precursors of SARS-CoV-2 has been reported here to provide necessary information, which may be helpful to understand the applicability of curcumin in the treatment against SARS-CoV-2.

In the present study, not only the interaction of the curcumin with precursors of SARS-CoV-2 but also its conformational flexibility has been monitored to get

the in-depth understanding related to the protein-ligand interaction. The study has been performed to monitor the distribution of electron density, dipole moment, atomic charge and atom-in-molecule (AIM) properties of curcumin in the gas phase as well as in the active sites of four different precursors related to SARS-CoV-2. The non-covalent interaction (NCI) analysis is performed for the visualization of weak interactions in the active sites. The NCI plot is efficient to study the macromolecular system effectively.

COMPUTATIONAL DETAIL

Molecular docking is the most famous tool to monitor the interaction of ligand and receptor.[21] It provides the useful information about the binding site of the protein used by the ligand to accommodate through various non-covalent interactions. The docking studies has been performed using computational software. AutoDock4 together with AutoGrid4 python programming-based tool has been used to study the molecular docking of curcumin with TMPRSS2, ACE2, PLpro and 3CLpro.[22-23] The docking uses the grid driven method to prepare grids around the protein and the lookup table for the simulation by calculating the energy keeping an atom as a probe on each of the grid points. The lookup table helps the simulation to effectively measure the binding energy of the conformers with the target protein. Further Lamarckian genetic algorithm has been used to search the lowest binding energy conformer associated in the local minima position close to the protein. AutoDock4 uses the semiempirical method to obtain the binding energies for the suitable conformers at the docking site of the protein in bound as well as unbound states. The study therefore provides interesting information about the reliable docking pose prediction for ligand protein interactions. PyMOL, LigPlot+ and Protein-ligand Interaction Profiler (PLIP) tools are used to draw the informative pictures of docking studies.[24-26] PLIP tool is also used here to identify the non-covalent interaction of curcumin with TMPRSS2, ACE2, PLpro and 3CLpro.

The efficacy of curcumin against the SARS-CoV-2 virus has been realized by studying the interaction of curcumin with TMPRSS2, ACE2, 3CLpro and PLpro. This interaction has been monitored using the docking studies. For these docking studies, crystal structures of TMPRSS2 (PDB ID: 1Z8A), ACE2 (PDB ID: 3D0G), PLpro (PDB: 3E9S), and 3CLpro (PDB ID: 3AW0) are used. These PDBs are obtained from Protein Data Bank (https://www.rcsb.org/).[27]

To understand the conformational flexibility of the curcumin, its diketone form in the gas phase is compared with the same obtained from the active sites of TMPRSS2, ACE2, PLpro and 3CLpro. Single point calculations are performed for curcumin obtained from active sites of TMPRSS2, ACE2, PLpro and 3CLpro whereas optimization has been performed to obtain the most stable geometry of curcumin in the gas phase at B3LYP/de2-TZVP level of theory. B3LYP is Becke's three-parameter exchange functional with the Lee-Yang-Parr correlation functional, which provides good result with reasonable error.[28] The def2-TZVP proposed by Ahlrichs–Weigend is triple-zeta valence with polarization basis set.[29] It provides better result than 6–311G**.[30-31] Furthermore, def2 basis sets are designed to deliver consistent accuracy for nearly all atoms up to radon.[30, 32] These calculations are performed using Turbo mole Version 7.6 ab initio quantum-chemical calculation software package.[33-34] The comparison has also been made based on the geometrical parameter, atomic charge, electron density, Laplacian of electron density, dipole moment and the energy gap between highest occupied and lowest unoccupied molecular orbitals. NCI and AIM analysis are performed using NCI Plot and Turbomole Version 7.6 software, respectively.[33-35]

RESULTS AND DISCUSSION

The docking studies of curcumin has been studied with TMPRSS2, ACE2, PLpro and 3CLpro, which are related to coronavirus 2 (SARS-CoV-2). For these docking studies, ten rotatable bonds of curcumin are used. The lowest binding energy docking pose of curcumin with TMPRSS2, ACE2, PLpro and 3CLpro are shown in Figure 1.

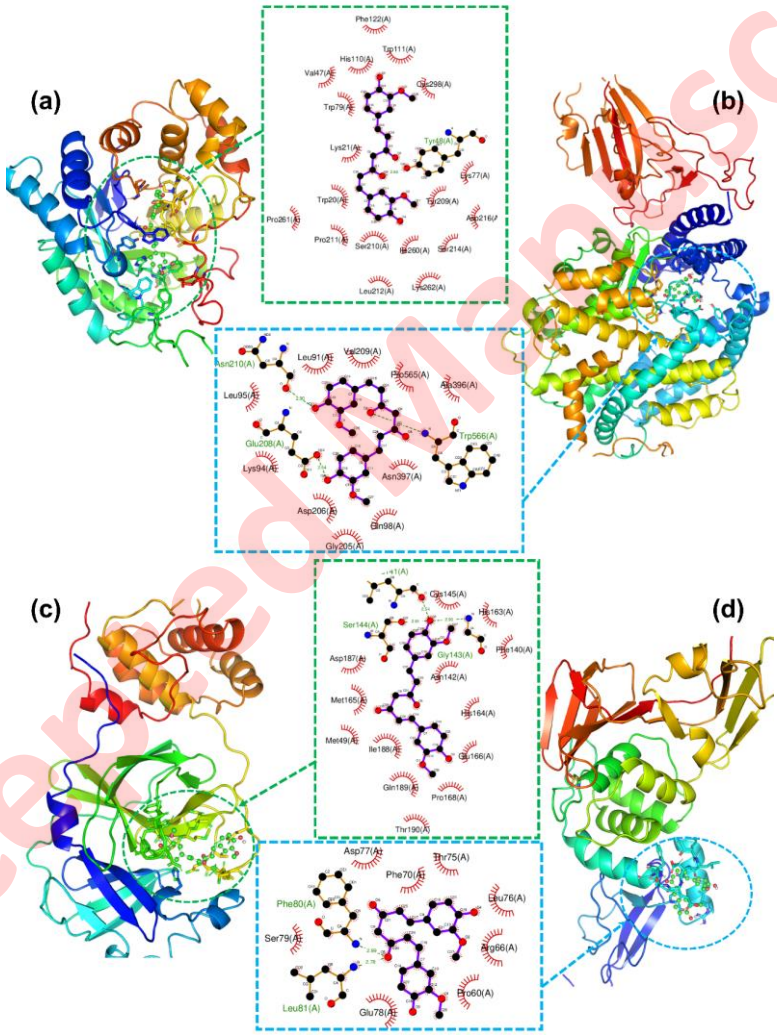

Figure 1. Lowest binding energy docking pose of curcumin in the (a) transmembrane serine protease 2 (TMPRSS2) PDB ID: 1Z8A, (b) angiotensin-converting enzyme 2 (ACE2) PDB ID: 3D0G, (c) 3-chymotrypsin-like protease (3CLpro) PDB ID: 3AW0 and (d) papain-like protease (PLpro) PDB ID: 3E9S

The lowest binding energy of curcumin with TMPRSS2, ACE2, PLpro and 3CLpro are -42.34, -28.53, -33.85, -31.33 kJ/mol, respectively. Interestingly, the most stable docking pose of curcumin has been observed with TMPRSS2. The detailed study of the four most stable docking poses of curcumin in TMPRSS2, ACE2, PLpro and 3CLpro has been reported in the supporting information. The ligand efficiency and the intermolecular energy of curcumin with TMPRSS2 are measured the highest whereas the tortional free energy is found the same for all four complexes formed after docking. Sametime, the inhibition efficiency of curcumin with TMPRSS2 (38.37 nM) is found the lowest compared to that with ACE2 (10.0 µM), PLpro (1.18 µM) and 3CLpro (3.22 µM).

Furthermore, the docking studies show that curcumin interacts with TMPRSS2 through both hydrogen bonding (H-bonding) and dispersion interactions. Amino acids LYS21, TYR48, TRP111 and LEU212 of Chain A interacts through H-bonding and the corresponding H-bonding distance is found 4.01, 3.15, 3.72 and 3.86 Å, respectively. Interestingly, the aromatic rings of amino acid TRP21 of chain A of TMPRSS2 and curcumin interact through π-π stacking interaction with an interplanar distance of 5.49 Å, the interaction is shown in Figure 1a. Several other amino acids interact through hydrophobic interactions. These interactions are shown in Figure 1a. Amino acids LYS94, GLN98, TYR196, GLU208 and TRP566 of chain A of ACE2 interact with curcumin through H-bonding and the corresponding H-bonding distances are 3.92, 3.84, 3.79, 2.54 and 2.99 Å, respectively whereas other interactions have been shown in Figure 1b. Interestingly, GLY143, SER144 and GLU189 of chain A of PLpro and ARG66, PHE80 and LEU81 of Chain A of 3CLpro interacts with curcumin through hydrogen bonding. The detailed chart of interactions in the lowest binding energy docking poses of curcumin with TMPRSS2, ACE2, PLpro and 3CLpro is shown in the supporting information. The Adaptive Poisson-Boltzmann Solver (ABPS), which provides the Poisson–Boltzmann electrostatic calculation, are also depicted in the supporting information, which shows the electrostatic interaction of curcumin with TMPRSS2, ACE2, 3CLpro and PLpro.

Amino acids GLY143, SER144 and GLN189 of chain A of PLpro interacts to curcumin through H-bonding with distance of 2.90, 2.58 and 2.56 Å, respectively. 2D and 3D representation of docking poses of curcumin with PLpro are shown in Figure 1c. Amino acids ARG66, PHE80 and LEU81 of chain A of 3CLpro interacts to curcumin through H-bonding with distance of 3.43, 2.99 and 2.78 Å, respectively (see Figure 1d).

Structural analysis

The optimized geometry of curcumin in the gas phase (I) at B3LYP/def2-TZVP level of theory and geometries of curcumin lifted from the lowest binding energy active sites of TMPRSS2 (IIa), ACE2 (IIb), 3CLpro (IIc) and PLpro (IId) are depicted in Figure 2 whereas the corresponding geometrical parameters are

tabulated in the supporting information. Curcumin is an interesting molecule connected through a long chain of multiple conjugated double bonds, which provides it structural flexibility to adjust in the active sites. Figure 2 shows a surprising glimpse of this structural flexibility of curcumin in various active sites. The geometry of curcumin bends a lot in the active site of ACE2 and PLpro in comparison to the geometry of gas phase and acquires U-shape. Interestingly, the study of geometrical parameters provides in-depth understanding about this.

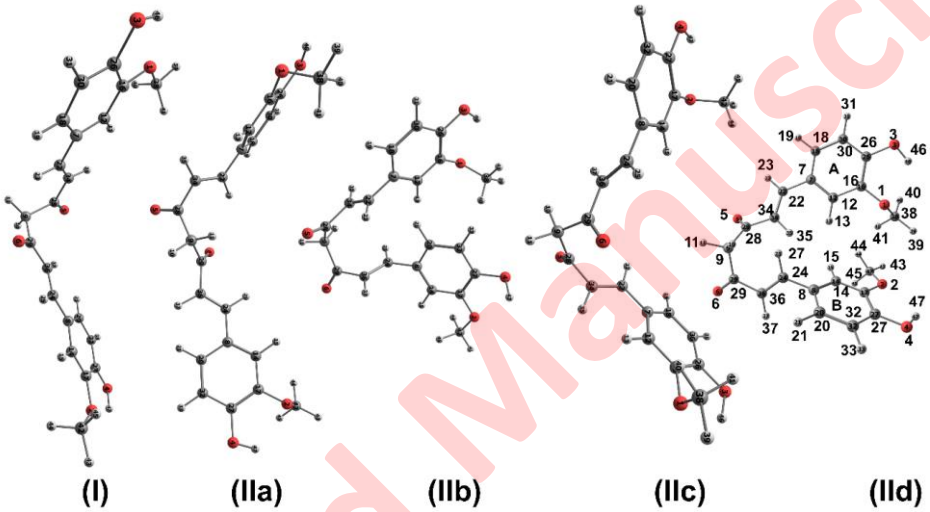

Figure 2. Optimized geometry (I) of curcumin in gas phase at B3LYP/def2-TZVP level of theory. Geometries of curcumin lifted from the active site of TMPRSS2 (IIb), ACE2 (IIb), 3CLpro (IIc) and PLpro (IId)

The bond length of ring C(sp^2) – C(sp^2) carbon bonds in curcumin in gas phase (I) and the same lifted from active sites (IIa, IIb, IIc, IId) are measured between 1.38-1.41 Å whereas the bond angles inside the rings are found between 118.3°-121.5°. A small change is reported in the geometrical parameters inside ring. The bond lengths of chain carbon bonds C8– C24, C36-C29, C28-C34 and C7-C22 are found to be increased by 0.02 Å in the active sites compared to that in the gas phase. The increase in bond length is attributed to intermolecular interaction with the amino acids in the active sites.

Interestingly, the major change is observed in the dihedral angles along the chain length in different forms of curcumin. Dihedral angles ∠C22-C34-C28-C9, ∠C34-C28-C9-C29, ∠C28-C9-C29-C36 and ∠C9-C29-C36-C24 in the form (I) are measured 5.2°, -80.3°, -67.5° and -177.3°, respectively. The same in the form (IIb) are -135.7°, 104.3°, -39.1° and -66.7°, respectively whereas the same in the form (IId) are -141.1°, -93.1°, 79.3° and -5.4°, respectively. The changes in the

dihedral angles are mainly responsible for the geometrical change to U-shape in IIb and IId forms, which can be observed in Figure 2.

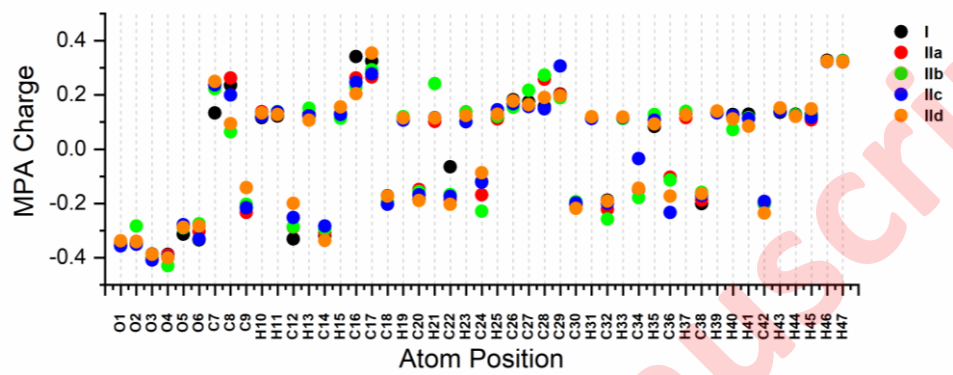

Figure 3. Mulliken population analysis (MPA) charges of curcumin in the gas phase and that lifted from the active site of TMPRSS2 (IIb), ACE2 (IIb), 3CLpro (IIc) and PLpro (IId)

Atomic charge

Mulliken population analysis (MPA) charges of curcumin in the gas phase and that lifted from the active site of TMPRSS2 (IIb), ACE2 (IIb), 3CLpro (IIc) and PLpro (IId) calculated at B3LYP/def2-TZVP level of theory and reported in Figure 3. The corresponding plot of Natural population analysis (NPA) charge along with detailed data is reported in the supporting information. The study depicts that MPA charges of hydroxyl oxygens O3 are -0.38681e, -0.39929e, -0.39646e, -0.40884e and -0.38819e for I, IIa, IIb, IIc and IId, respectively. Similarly, MPA charges of hydroxyl oxygens O4 are -0.38775e, -0.38995e, -0.42946e, -0.39773e and -0.39995e for I, IIa, IIb, IIc and IId, respectively. It shows that MPA charge of hydroxy oxygen increases on binding with amino acids in the active site of receptor in comparison to that in the gas phase (I). Interestingly the MPA charges of hydroxyl oxygen O3 and O4 are found lower than carbonyl oxygens, O5 and O6. Sametime the carbon atom attached to the electronegative oxygens O3, O4, O5 and O6 are C26, C27, C28 and C29, respectively and the MPA charges of these carbons are found higher. This is prominently reported in case of NPA charges (see Figure S7). NPA charges for hydroxyl oxygen O3 and O4 are less than that for carbonyl oxygen O5 and O6 for all forms of curcumin whereas an increase in NPA charges is also reported for O3, O4, O5 and O6 in case of curcumin lifted from the active sites. Overall, the comparison of atomic charges (MPA and NPA) nicely helps to understand the interaction of curcumin with TMPRSS2, ACE2, 3CLpro and PLpro.

AIM analysis

Electron density ρ_{bcp} (r) and Laplacian of electron density $\nabla^2\rho_{bcp}$ (r) of curcumin in the gas phase (I) and that lifted from the active site of TMPRSS2 (IIa), ACE2 (IIb), 3CLpro (IIc) and PLpro (IId) are studied at B3LYP/def2-TZVP level of theory and graphically represented in Figure 4. The corresponding detailed report and figure have been added in the supporting information. An average of ρ_{bcp} (r) at the bond critical points (BCP) of carbon bonds in the two aromatic rings of curcumin (I) are 0.3191 / 0.3190 a.u. whereas the same of curcumin in the form IIa, IIb, IIc and IId are 0.3213 / 3214, 0.3207 / 0.3207, 0.3215 / 0.3210 and 0.3219 / 0.3202 a.u., respectively. Interestingly, the ρ_{bcp} (r) at ring critical points (RCPs) of two aromatic rings of curcumin in I form are 0.0229 / 0.0230 a.u. whereas the same for curcumin in IIa, IIc, IIc and IId are 0.0233 / 0.0232, 0.0231/ 0.0232, 0.0231 / 0.0232 and 0.0233 / 0.0231 a.u., respectively. It shows that the electron densities at the curcumins in the forms IIa, IIb, IIc and IId increase in comparison to that in gas phase i.e., isolated form (I) due to interaction with amino acids present in the docking site.

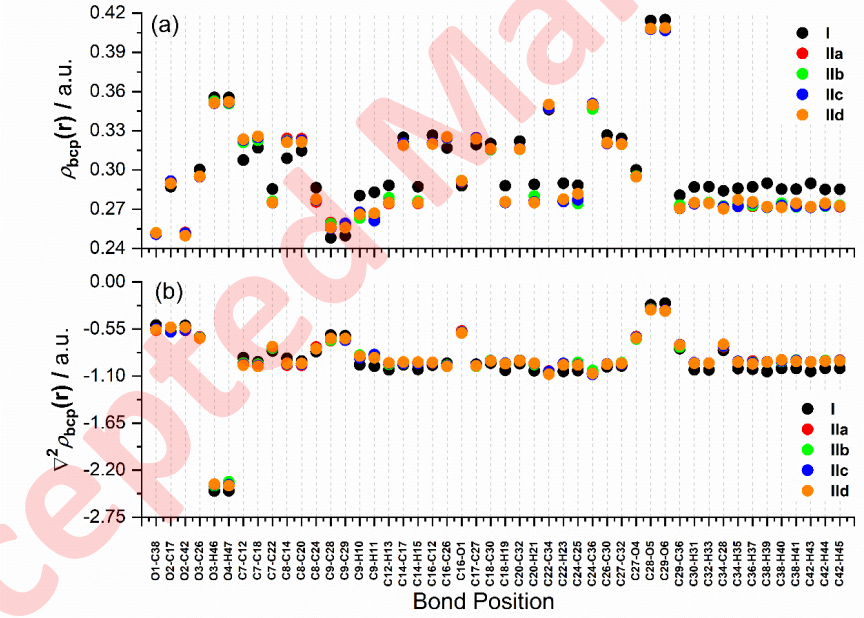

Figure 4. Plot of (a) electron density ρ_{bcp} (r) and (b) Laplacian of electron density $\nabla^2\rho_{bcp}$(r) of curcumin in the gas phase and the same lifted from the active site of TMPRSS2 (IIa), ACE2 (IIb), 3CLpro (IIc) and PLpro (IId).

The ρ_{bcp} (r) of alcoholic bonds O3-H46 and O4-H47 are measured 0.3555 / / 0.3555 a.u. in form (I) whereas that are in curcumin in the form IIa, IIb, IIc and IId are 0.3523 / 0.3520, 0.3525 / 0.3507, 0.3510 / 0.3516 and 0.3514 / 0.3521 a.u., respectively. A jump in ρ_{bcp} (r) of ketonic bond C28-O5 and C29-O6 are measured

0.4143 / 0.415 a.u. in form (I) whereas the same in curcumin lifted from the form IIa, IIb, IIc and IId are 0.4078/ 0.4075, 0.4078 /0.4076, 0.4077/ 0.4068 and 0.4082/ 0.4087 a.u., respectively. Thus, the ρ_{bcp} (r) of alcoholic and ketonic bonds of curcumin decreases in the active site compared to that in gas phase by 0.003 and 0.007 a.u. The H-bonding interaction is found responsible for this difference.

Sametime $\nabla^2\rho_{bcp}$(r) for the hydroxyl groups of curcumin in the forms IIa, IIb, IIc and IId are higher than that in the gas phase (I). The difference is attributed to H-bonding interaction. The comparison of ρ_{bcp} (r) and $\nabla^2\rho_{bcp}$ (r) of the ketonic groups (C29-O6 and C28-O5) in the four different forms of curcumin defines its interaction with amino acids in the docking site.

HOMO-LUMO band gap and dipole moment measurements

The geometries of curcumin in gas phase are optimized at B3LYP/def2-TZVP level of theory while single point calculations are performed for IIa, IIb, IIc and IId at same level of theory. HOMO energy gives the impression of ionization potential relating the ability to donate an electron while LUMO energy directly correlates with electron affinity relating the ability to accept an electron. Thus HOMO-LUMO energy gap provides the information about the molecular stability. As HOMO-LUMO energy gap for a molecule decreases the polarizability and the reactivity of the molecule increases. The HOMO-LUMO calculations are performed and reported 3.699 eV in the gas phase whereas the same obtained for IIa, IIb, IIc and IId are 4.367, 4.392, 3.714 and 4.058 eV, respectively. The band gap is found lowest at the gas phase and the band gap for IIc is measured close to gas phase but high value of band gap is measured for IIa and IIb.

Dipole moments (μ) has also calculated for all the forms of curcumin at B3LYP/def2-TZVP level of theory and reported in the supporting information. The dipole moment of curcumin in the gas phase (I) is calculated 3.26 D whereas dipole moments of IIa, IIb, IIc and IId are 7.022, 4.147, 4.429 and 6.8 D, respectively. The dipole moments of IIa, IIb, IIc and IId is greater than that of I, which is attributed to intermolecular interaction as well as charge distribution present close to curcumin in the active sites. Interestingly, the dipole moment of IIa is found higher than that of IIb, IIc and IId. Interestingly, the binding energy for the most preferable docking pose of curcumin with TMPRSS2 (-42.34 kJ/mol) is found lower than that in case of ACE2, PLpro and 3CLpro.

Non-covalent interaction (NCI) plot

NCI plot is helpful to understand the various non-covalent interactions present in the macromolecule. Yang and coworkers implemented reduced density gradient ($RDG=|\nabla_\rho|/2(3\pi^2)^{1/3}\rho^{4/3}$) to measure the parameters related to the non-covalent interactions in NCI Plot.[35] Therefore, NCI plot is used to monitor the interaction of curcumin in the active site of TMPRSS2, ACE2, PLpro and 3CLpro. The lowest binding energy docking sites are chosen for this purpose. The closest interaction

within 3.5 Å was selected using Pymol software. The selected residues from TMPRSS2, ACE2, PLpro and 3CLpro along with curcumin are used for NCI Plot. Figure 5 shows the NCI plot and underlying interactions for curcumin with the TMPRSS2, ACE2, PLpro and 3CLpro.

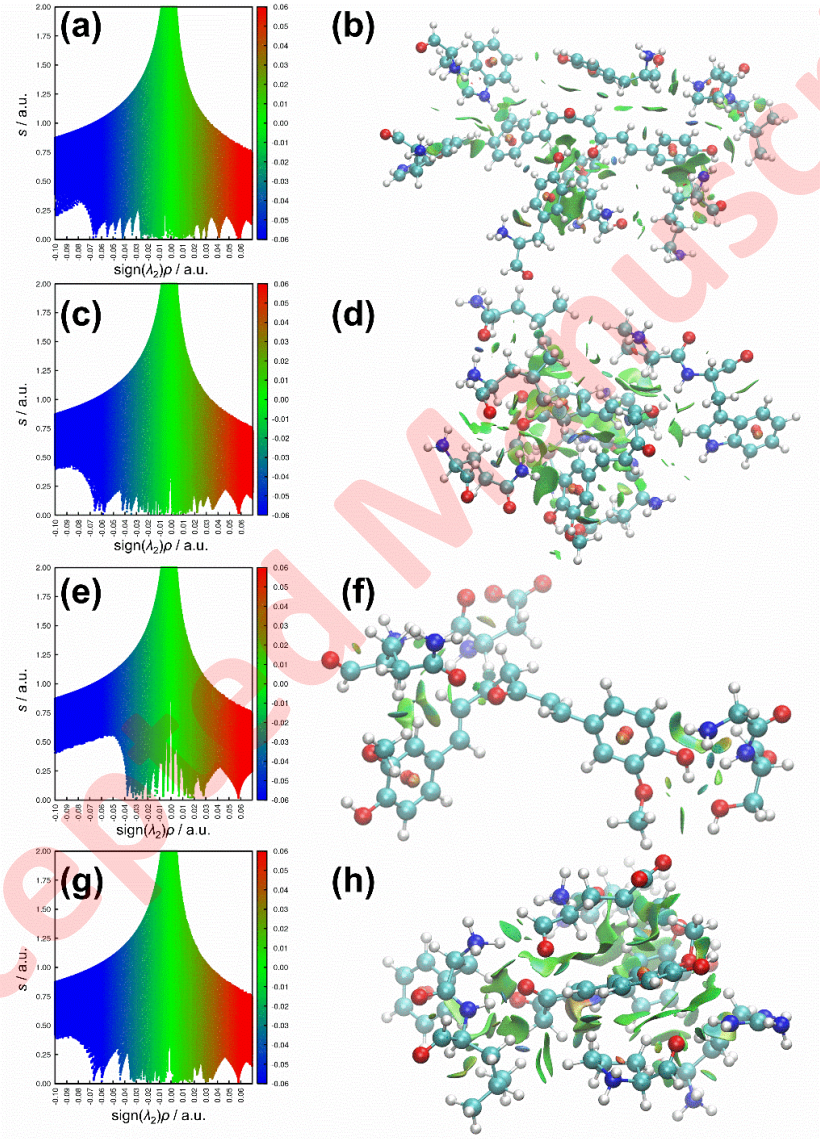

Figure 5. RDG plot of NCI analysis for docking poses of curcumin with TMPRSS2, ACE2, 3CLpro and PLpro are plotted in (a), (c), (e) and (g), respectively whereas its corresponding isosurface extractions of RDG plots of NCI analysis are represented in (b), (d), (f) and (h), respectively

The coloring scheme used to discuss the isosurfaces is as follows. The blue colour indicates the strong attractive interaction. The green color indicates the interactions having intermediate strength such as H-bonding, π-π, van der Waals interactions (vdW). The red colour represents the repulsive forces. A mixture of green and blue has been mostly seen in the NCI plot, which also represents electrostatic as well as dispersion interactions. Figure 5(a, c, e and f) depict RDG plots of NCI analysis of docking poses of curcumin with TMPRSS2, ACE2, PLpro and 3CLpro. These plots show mostly blue and green colours indicating that the main contribution to the binding strength is originated from H-bonding and vdW interactions. The same is also confirmed through PLIP analysis.[26] The extended plots are separately shown in the supporting information for clear visibility.

Figure 5b shows the isosurface extraction of NCI analysis showing H-bonding interaction between C=O and O-H groups of curcumin with O-H group of tyrosine and N-H group of leucine, respectively. Sametime, curcumin also interacts with TRP20, TRP79, TRP111, TYR209 through hydrogen bounding interaction in the active site of TMPRSS2P. The study supports the interactions shown in Figure 1. Figure 5(c, d) show the NCI plot and its isosurface extractions of the intermolecular interactions between curcumin and amino acids present in the active site of ACE2. Figure 5f shows that the C=O group of curcumin interacts with N-H groups of LEU81 and PHE80 of chain A. Thus, NCI plots provided in-depth understanding of intermolecular interaction present between ligand and receptor.

CONCLUSIONS

The study of curcumin with transmembrane serine protease 2 (TMPRSS2), angiotensin-converting enzyme 2 (ACE2), 3-chymotrypsin-like protease (3CLpro) and papain-like protease (PLpro) are performed using molecular docking and detailed quantum chemistry calculation. Quantum chemistry calculation provides in-depth quantitative information regarding the underlying interactions. Curcumin has multiple single bonds providing it freedom to adjust into the lowest binding energy pockets after geometrical rearrangements. The study of curcumin in the active sites has been performed through calculation of geometrical parameters, atomic charges, electron density, Laplacian of electron density, dipole moments, energy gap between highest occupied and lowest unoccupied molecular orbitals as well as NCI analysis. The study revealed that curcumin can acts as a potential multiple-target inhibitors against SARS-CoV-2.

Acknowledgements: I would like to thank Magadh University, Bodh Gaya-824234, Bihar, India for providing lab facility to perform research. Science and Engineering Research Board, Department of Science and Technology (DST), Ministry of Science and Technology, India (Grant No. SRG/2019/002284) has been acknowledged for financial support.

Supplementary material to this paper is available electronically from https://www.shd-pub.org.rs/index.php/JSCS/article/view/12081, or from the corresponding author on request.

ИЗВОД

КУРКУМИН КАО ПОТЕНЦИЈАЛНИ ИНХИБИТОР ВИШЕСТРУКИХ МЕТА ПРОТИВ SARS-CoV-2 ИНФЕКЦИЈЕ: ДЕТАЉНО ПРОУЧАВАЊЕ ИНТЕРАКЦИЈЕ КОРИШЋЕЊЕМ КВАНТНО-ХЕМИЈСКИХ ИЗРАЧУНАВАЊА

SUMIT KUMAR

Department of Chemistry, Magadh University, Bodh Gaya-824234, Bihar, India

Куркумин је једно од значајних природних једињења које има више медицинских особина као што су антивирусне, антиоксидантне као и протуупалне особине. SARS-CoV-2 се појавио као заразни вирус, који озбиљно заражава велике групе становништва у свету. Било је неколико покушаја да се направе нова антивирусна једињења, али то остаје као изазов чак и након строгих трајала. Природни производ, куркумин, може се користити као алтернатива антивирусних једињења за SARS-CoV-2. Његово дејство против SARS-CoV-2 већ је истакнуто у литератури. Али до данас није није саопштено о квантитативном проучавању његове интеракције са различитим прекурсорима SARS-CoV-2. Овај чланак саопштава о интеракцији куркумина са ангиотензин-конвертујућим ензимом2, транс-мембранском серин протеазом 2, на 3-химотрипсин налик протеазом и на папаин налик протеазом, помоћу молекулског докинга и квантно хемијских израчунавања, да би постигли квантитативно разумевање основа интеракција. Овде смо постигли да и конформациона флексибилност куркумина буде осветљена, што помаже да га се смести у четири различита места за доковање. Студија је изведена коришћењем израчунавања геометријских параметара, атомсих наелектрисања, густине електрона, Лапласијана електронске густине, диполног момента и енергетског јаза између највише попуњене и најниже незаузете молекулске орбитале. Урађена је анализа не-ковалентних интеракција (NCI) да би се визуализовале слабе интеракције присутне у активним местима. Комбиновање молекулског докинга и детаљних квантно хемијских израчунавања показује да куркумин може бити прихваћен као потенцијални инхибитор вишеструких мета против SARS-CoV-2.

(Примљено 21. септембра; ревидирано 21. новембра; прихваћено 9. децембра 2022.)

REFERENCES

1. M. Cevik, M. Tate, O. Lloyd, A. E. Maraolo, J. Schafers, A. Ho, *Lancet Microbe* **2** (2021) e13 (http://dx.doi.org/10.1016/S2666-5247(20)30172-5)
2. L. M. Mattio, G. Catinella, A. Pinto, S. Dallavalle, *Eur. J. Med. Chem.* **202** (2020) 112541 (http://dx.doi.org/10.1016/j.ejmech.2020.112541)
3. L. T. Lin, W. C. Hsu, C. C. Lin, *J. Tradit. Complement. Med.* **4** (2014) 24 (http://dx.doi.org/10.4103/2225-4110.124335)
4. F. A. C. Rocha, M. R. de Assis, *Phytother. Res.* **34** (2020) 2085 (http://dx.doi.org/10.1002/ptr.6745)
5. F. Zahedipour, S. A. Hosseini, T. Sathyapalan, M. Majeed, T. Jamialahmadi, K. Al-Rasadi, M. Banach, A. Sahebkar, *Phytother. Res.* **34** (2020) 2911 (http://dx.doi.org/10.1002/ptr.6738)
6. V. K. Soni, A. Mehta, Y. K. Ratre, A. K. Tiwari, A. Amit, R. P. Singh, S. C. Sonkar, N. Chaturvedi, D. Shukla, N. K. Vishvakarma, *Eur. J. Pharmacol.* **886** (2020) 173551 (http://dx.doi.org/10.1016/j.ejphar.2020.173551)
7. F. Babaei, M. Nassiri-Asl, H. Hosseinzadeh, *Food Sci. Nutr.* **8** (2020) 5215 (http://dx.doi.org/10.1002/fsn3.1858)

8. R. K. Thimmulappa, K. K. Mudnakudu-Nagaraju, C. Shivamallu, K. J. T. Subramaniam, A. Radhakrishnan, S. Bhojraj, G. Kuppusamy, *Heliyon* **7** (2021) e06350 (http://dx.doi.org/10.1016/j.heliyon.2021.e06350)
9. A. Saeedi-Boroujeni, M. R. Mahmoudian-Sani, M. Bahadoram, A. Alghasi, *Basic Clin. Pharmacol. Toxicol.* **128** (2021) 37 (http://dx.doi.org/10.1111/bcpt.13503)
10. N. Chainani-Wu, *J. Altern. Complement. Med.* **9** (2003) 161 (http://dx.doi.org/10.1089/107555303321223035)
11. Y. Huang, C. Yang, X. F. Xu, W. Xu, S. W. Liu, *Acta Pharmacol. Sin.* **41** (2020) 1141 (http://dx.doi.org/10.1038/s41401-020-0485-4)
12. H. Zhang, J. M. Penninger, Y. Li, N. Zhong, A. S. Slutsky, *Intensive Care Med.* **46** (2020) 586 (http://dx.doi.org/10.1007/s00134-020-05985-9)
13. A. Domling, L. Gao, *Chem* **6** (2020) 1283 (http://dx.doi.org/10.1016/j.chempr.2020.04.023)
14. M. Hoffmann, H. Kleine-Weber, S. Schroeder, N. Kruger, T. Herrler, S. Erichsen, T. S. Schiergens, G. Herrler, N. H. Wu, A. Nitsche, M. A. Muller, C. Drosten, S. Pohlmann, *Cell* **181** (2020) 271 (http://dx.doi.org/10.1016/j.cell.2020.02.052)
15. A. B. Jena, N. Kanungo, V. Nayak, G. B. N. Chainy, J. Dandapat, *Sci. Rep.* **11** (2021) 2043 (http://dx.doi.org/10.1038/s41598-021-81462-7)
16. A. C. Walls, Y. J. Park, M. A. Tortorici, A. Wall, A. T. McGuire, D. Veesler, *Cell* **181** (2020) 281 (http://dx.doi.org/10.1016/j.cell.2020.02.058)
17. N. Barretto, D. Jukneliene, K. Ratia, Z. Chen, A. D. Mesecar, S. C. Baker, *J. Virol.* **79** (2005) 15189 (http://dx.doi.org/10.1128/jvi.79.24.15189-15198.2005)
18. M. L. DeDiego, E. Alvarez, F. Almazán, M. T. Rejas, E. Lamirande, A. Roberts, W.-J. Shieh, S. R. Zaki, K. Subbarao, L. Enjuanes, *J. Virol.* **81** (2007) 1701 (http://dx.doi.org/10.1128/JVI.01467-06)
19. L. Kuo, P. S. Masters, *J. Virol.* **77** (2003) 4597 (http://dx.doi.org/10.1128/JVI.77.8.4597-4608.2003)
20. J. Ortego, J. E. Ceriani, C. Patino, J. Plana, L. Enjuanes, *Virology* **368** (2007) 296 (http://dx.doi.org/10.1016/j.virol.2007.05.032)
21. X. Y. Meng, H. X. Zhang, M. Mezei, M. Cui, *Curr. Comput. Aided Drug Des.* **7** (2011) 146 (http://dx.doi.org/10.2174/157340911795677602)
22. G. M. Morris, R. Huey, W. Lindstrom, M. F. Sanner, R. K. Belew, D. S. Goodsell, A. J. Olson, *J. Comput. Chem.* **30** (2009) 2785 (http://dx.doi.org/10.1002/jcc.21256)
23. M. F. Sanner, *J. Mol. Graph. Model.* **17** (1999) 57 (http://dx.doi.org/10.1016/S1093-3263(99)99999-0)
24. R. A. Laskowski, M. B. Swindells, *J. Chem. Inf. Model.* **51** (2011) 2778 (http://dx.doi.org/10.1021/ci200227u)
25. A. C. Wallace, R. A. Laskowski, J. M. Thornton, *Protein Eng.* **8** (1995) 127 (http://dx.doi.org/10.1093/protein/8.2.127)
26. M. F. Adasme, K. L. Linnemann, S. N. Bolz, F. Kaiser, S. Salentin, V. J. Haupt, M. Schroeder, *Nucleic Acids Res.* **49** (2021) W530 (http://dx.doi.org/10.1093/nar/gkab294)
27. H. M. Berman, J. Westbrook, Z. Feng, G. Gilliland, T. N. Bhat, H. Weissig, I. N. Shindyalov, P. E. Bourne, *Nucleic Acids Res.* **28** (2000) 235 (http://dx.doi.org/10.1093/nar/28.1.235)
28. M. D. Wodrich, C. Corminboeuf, P. v. R. Schleyer, *Org. Lett.* **8** (2006) 3631 (http://dx.doi.org/10.1021/ol061016i)
29. F. Weigend, R. Ahlrichs, *Phys. Chem. Chem. Phys.* **7** (2005) 3297 (http://dx.doi.org/10.1039/B508541A)

30. F. Weigend, *Phys. Chem. Chem. Phys.* **8** (2006) 1057 (http://dx.doi.org/10.1039/B515623H)
31. X. Xu, D. G. Truhlar, *J. Chem. Theory Comput.* **7** (2011) 2766 (http://dx.doi.org/10.1021/ct200234r)
32. J. Zheng, X. Xu, D. G. Truhlar, *Theor. Chem. Acc.* **128** (2011) 295 (http://dx.doi.org/10.1007/s00214-010-0846-z)
33. F. Furche, R. Ahlrichs, C. Hättig, W. Klopper, M. Sierka, F. Weigend, *Wiley Interdiscip. Rev. Comput. Mol. Sci.* **4** (2014) 91 (http://dx.doi.org/10.1002/wcms.1162)
34. C. Steffen, K. Thomas, U. Huniar, A. Hellweg, O. Rubner, A. Schroer, *J. Comput. Chem.* **31** (2010) 2967 (http://dx.doi.org/10.1002/jcc.21576)
35. E. R. Johnson, S. Keinan, P. Mori-Sanchez, J. Contreras-Garcia, A. J. Cohen, W. Yang, *J. Am. Chem. Soc.* **132** (2010) 6498 (http://dx.doi.org/10.1021/ja100936w).

Journal of the Serbian Chemical Society
JSCS-info@shd.org.rs • www.shd.org.rs/JSCS
J. Serb. Chem. Soc. **00(0)** S1-S17 (2022) *Supplementary material*

SUPPLEMENTARY MATERIAL TO

Curcumin as a potential multiple-target inhibitor against SARS-CoV-2 Infection: A detailed interaction study using quantum chemical calculations

SUMIT KUMAR *

Department of Chemistry, Magadh University, Bodh Gaya-824234, Bihar, India

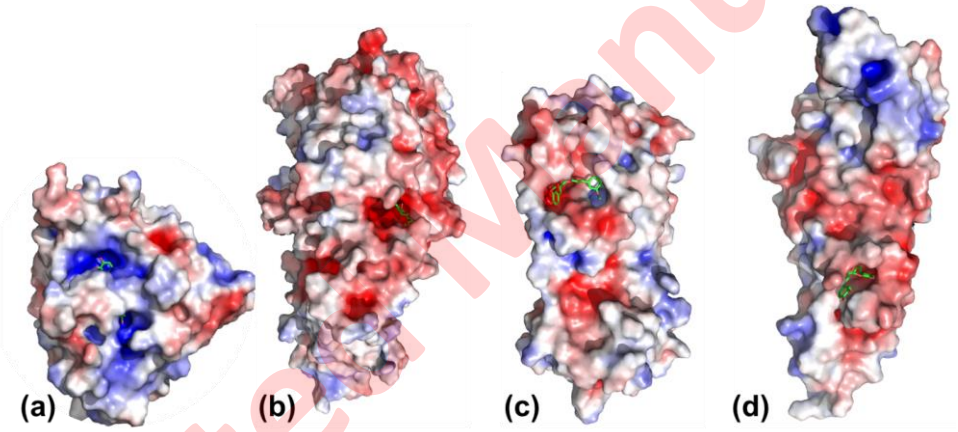

Figure S-1. Adaptive Poisson-Boltzmann Solver (ABPS) plots of the lowest binding energy docking site for the electrostatic interaction of curcumin with (a) TMPRSS2, (b) ACE2, (c) 3CLpro and (d) PLpro.

* Corresponding author E-mail: sumitkrmgr@gmail.com

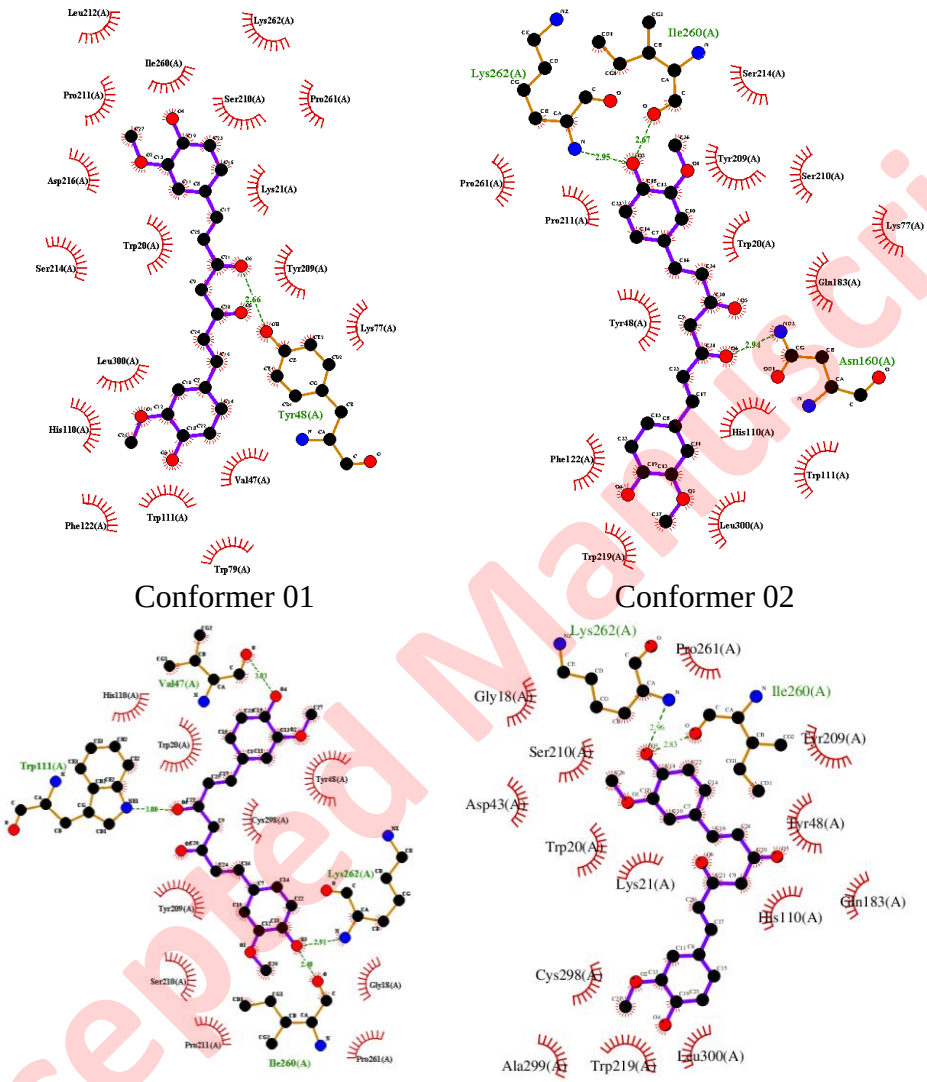

Figure S-2. The four most preferred docking poses of curcumin in the transmembrane serine protease 2 (TMPRSS2) PDB ID: 1Z8A

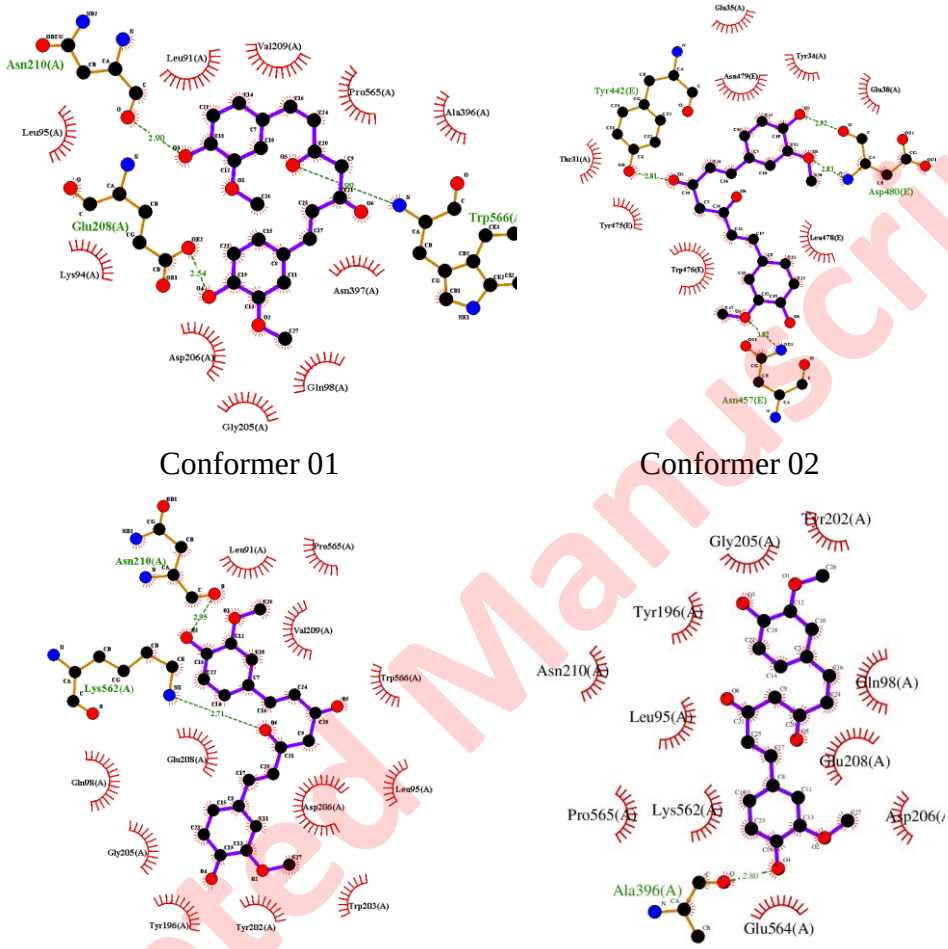

Conformer 01 Conformer 02

Conformer 03 Conformer 04

Figure S-3. The four most preferred docking poses of curcumin in the angiotensin-converting enzyme 2 (ACE2) PDB ID: 3D0G

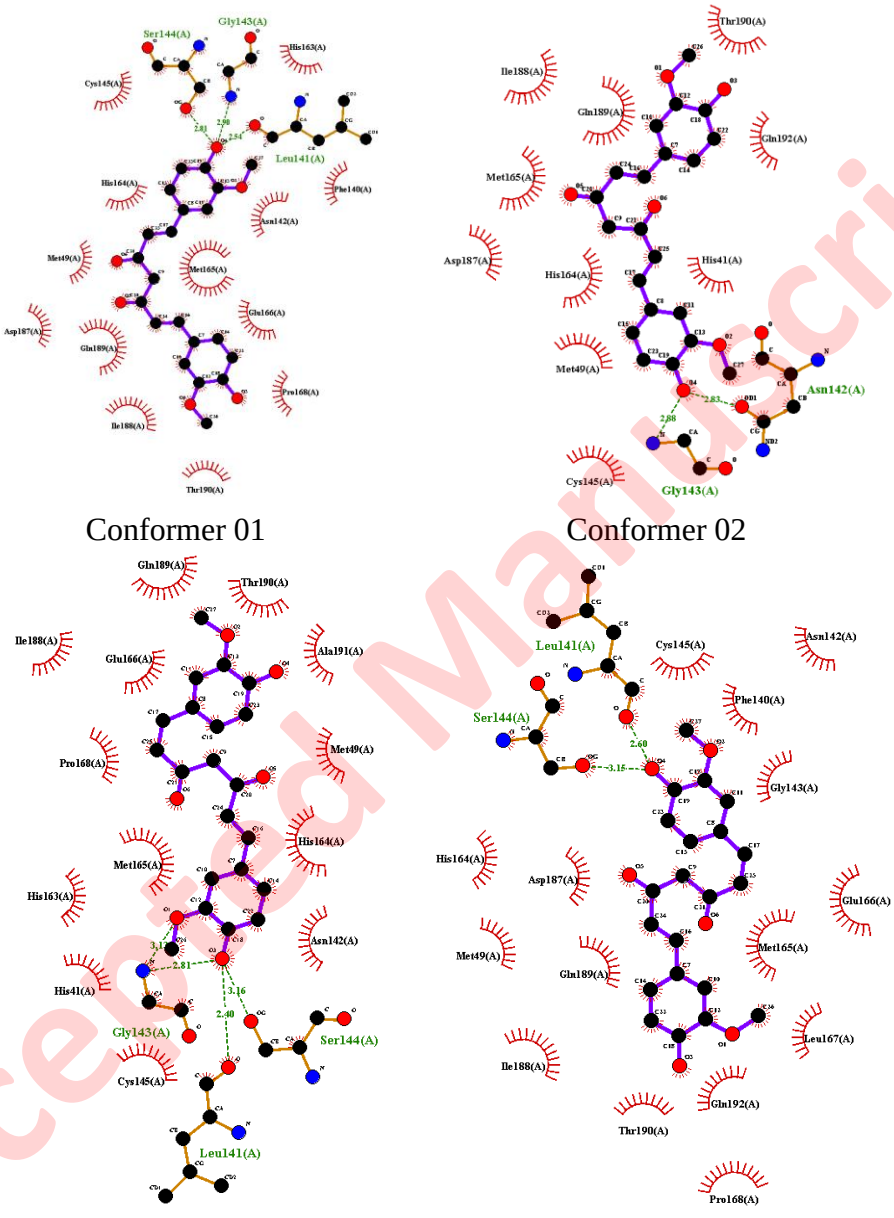

Figure S-4. The four most preferred docking poses of curcumin in the 3-chymotrypsin-like protease (3CLpro) PDB ID: 3AW0

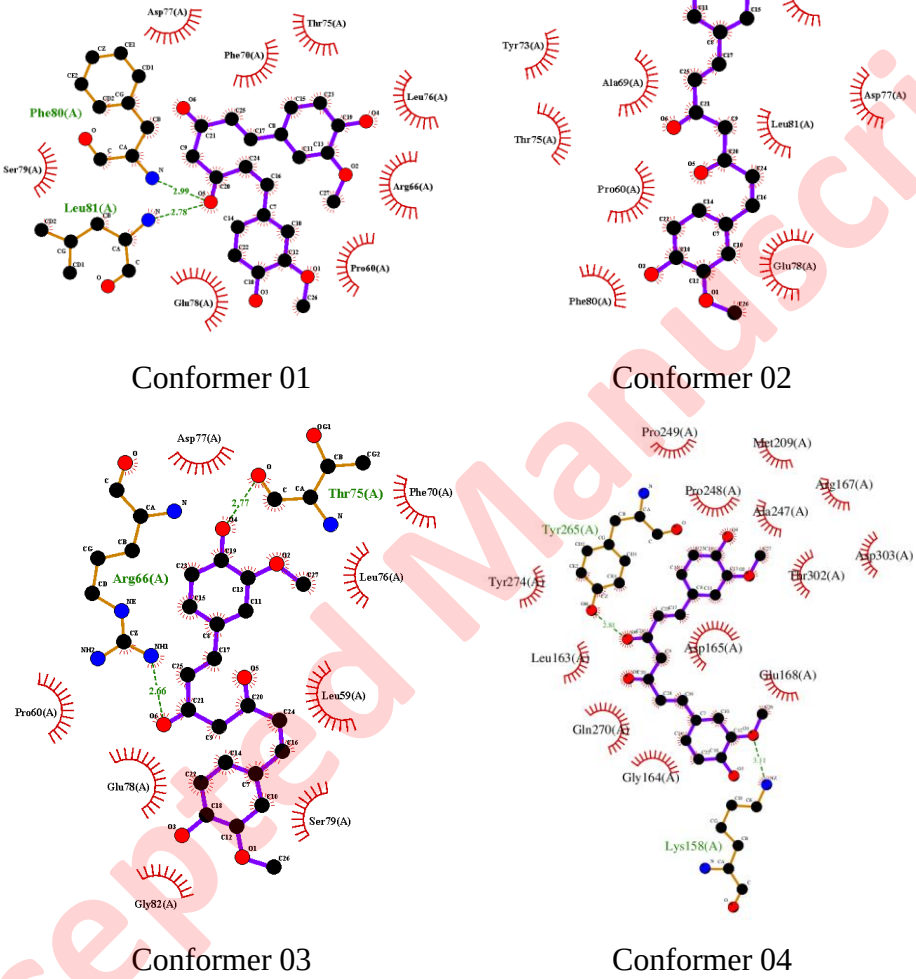

Conformer 01 Conformer 02

Conformer 03 Conformer 04

Figure S-5. The four most preferred docking poses of curcumin in the papain-like protease (PLpro) PDB ID: 3E9S

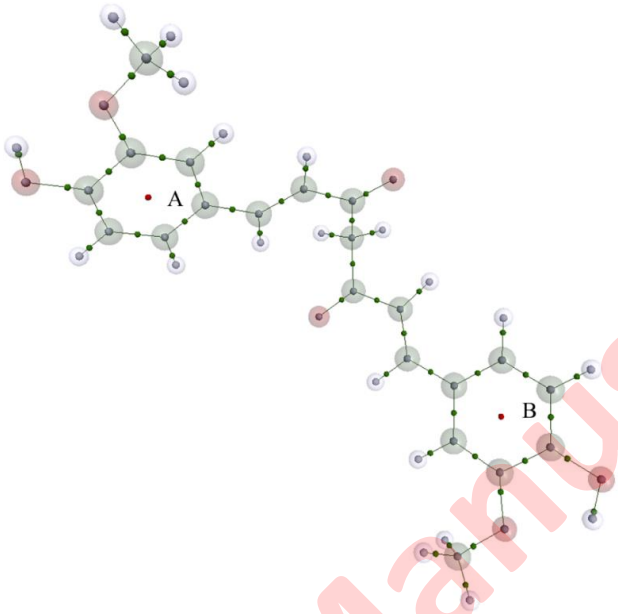

Figure S-6. Bond critical points (BCP) and ring critical points (RCPs) for curcumin in the gas phase obtained from AIM analysis at B3LYP/def2-TZVP level of theory

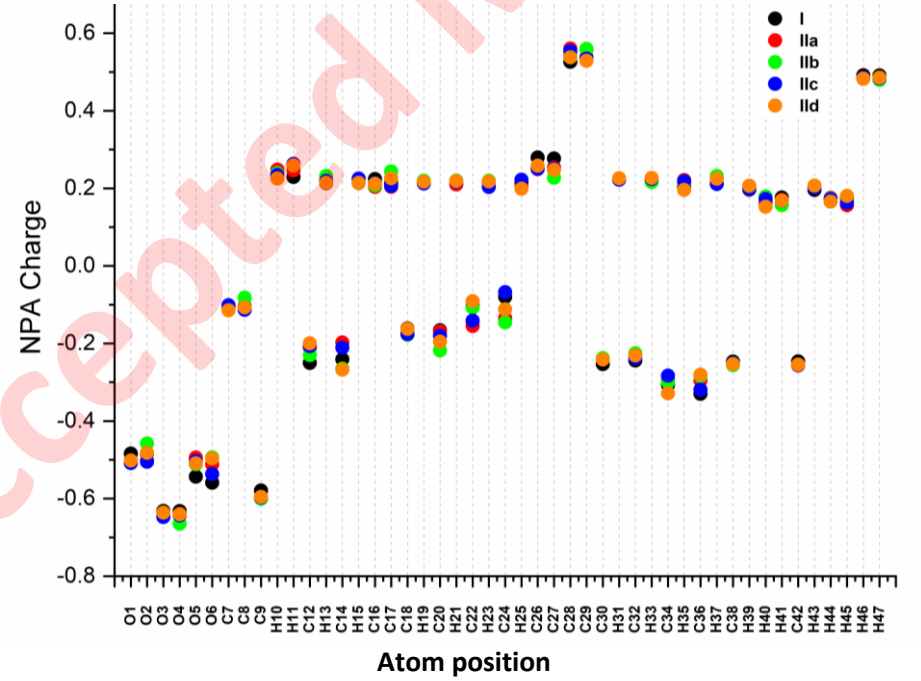

Figure S-7. Natural population analysis (NPA) charges of curcumin in the gas phase and that lifted from the active site of TMPRSS2 (IIb), ACE2 (IIb), 3CLpro (IIc) and PLpro (IId)

Table S-I. Estimated free energy of binding along with its subsidiary components and estimated inhibition constants for the four most preferred docking sites of curcumin in the transmembrane serine protease 2 (TMPRSS2) PDB ID: 1Z8A.

Receptor	Conformer 01	Conformer 02	Conformer 03	Conformer 04
Binding energy, kJ/mol	-42.34	-42.09	-41.97	-41.92
Inhibition constant, nM	38.37	42.32	44.57	45.47
Total intermolecular energy, kJ/mol	-54.43	-54.56	-54.43	-54.39
Total internal energy, kJ/mol	-8.74	-6.40	-5.52	-6.32
Torsional free energy, kJ/mol	12.47	12.47	12.47	12.47
Unbound system's energy, kJ/mol	-8.74	-6.40	-5.52	-6.32
Cluster RMSD, Å	0.00	1.29	0.00	0.79
Reference RMSD, Å	24.81	23.14	23.80	23.34

Table S-II. Estimated free energy of binding along with its subsidiary components and estimated inhibition constants for the four most preferred docking sites of curcumin in the angiotensin-converting enzyme 2 (ACE2) PDB ID: 3D0G.

Receptor	Conformer 01	Conformer 02	Conformer 03	Conformer 04
Binding energy, kJ/mol	-28.53	-27.24	-26.65	-25.65
Inhibition constant, µM	10.00	16.87	21.43	32.23
Total intermolecular energy, kJ/mol	-41.00	-39.71	-39.12	-38.12
Total internal energy, kJ/mol	-10.08	-10.88	-8.37	-9.00
Torsional free energy, kJ/mol	12.47	12.47	12.47	12.47
Unbound system's energy, kJ/mol	-10.08	-10.88	-8.37	-9.00
Cluster RMSD, Å	0.00	0.00	0.00	0.00
Reference RMSD, Å	102.60	127.25	104.15	104.66

Table S-III. Estimated free energy of binding along with its subsidiary components and estimated inhibition constants for the four most preferred docking sites of curcumin in the 3-chymotrypsin-like protease (3CLpro) PDB ID: 3AW0

Receptor	Conformer 01	Conformer 02	Conformer 03	Conformer 04
Binding energy, kJ/mol	-33.85	-32.05	-30.12	-29.71
Inhibition constant, µM	1.18	2.41	5.27	6.21
Total intermolecular energy, kJ/mol	-46.32	-44.56	-42.59	-42.22
Total internal energy, kJ/mol	-9.16	-9.50	-6.53	-9.62
Torsional free energy, kJ/mol	12.47	12.47	12.47	12.47
Unbound system's energy, kJ/mol	-9.16	-9.50	-6.53	-9.62
Cluster RMSD, Å	0.00	1.73	1.65	1.95
Reference RMSD, Å	42.05	42.92	42.20	41.44

Table SIV. Estimated free energy of binding along with its subsidiary components and estimated inhibition constants for the four most preferred docking sites of curcumin in the papain-like protease (PLpro) PDB ID: 3E9S.

Receptor	Conformer 01	Conformer 02	Conformer 03	Conformer 04
Binding energy, kJ/mol	-31.33	-30.33	-29.71	-27.36
Inhibition constant, µM	3.22	4.84	6.26	16.02
Total intermolecular energy, kJ/mol	-43.81	-42.84	-42.17	-39.87
Total internal energy, kJ/mol	-10.92	-10.71	-9.41	-8.62
Torsional free energy, kJ/mol	12.47	12.47	12.47	12.47
Unbound system's energy, kJ/mol	-10.92	-10.71	-9.41	-8.62
Cluster RMSD, Å	0.00	0.00	0.00	0.00
Reference RMSD, Å	31.12	30.86	29.67	43.00

Table S-V. List of interactions present in the lowest binding energy active site of curcumin with TMPRSS2 (PDB ID: 1Z8A), ACE2 (PDB ID: 3D0G), 3CLpro (PDB ID: 3AW0) and PLpro (PDB ID: 3E9S). These interactions are obtained from PLIP analysis

Receptor	Residues number	Residue	Curcumin	Distance, Å	Angle, °	Types
TMPRSS2P	21A	LYS	O2	4.01	133	H-bond
	48A	TYR	O5	3.15	109	H-bond
	111A	TRP	O1	3.72	112	H-bond
	212A	LEU	O4	3.86	126	H-bond
	20A	TRP	-	5.49	-	π-stack
ACE2	94A	LYS	O3	3.92	143	H-bond
	98A	GLN	O1	3.84	135	H-bond
	196A	TYR	O2	3.79	120	H-bond
	208A	GLU	O4	2.54	126	H-bond
	566A	TRP	O5	2.99	162	H-bond
PLpro	143A	GLY	O4	2.9	122	H-bond
	144A	SER	O4	2.58	122	H-bond
	144A	SER	O4	2.81	146	H-bond
	189A	GLN	O6	2.56	162	H-bond
3CLpro	66A	ARG	O1	3.43	116	H-bond
	80A	PHE	O5	2.99	115	H-bond
	81A	LEU	O5	2.78	168	H-bond

Table S-VI. Coordinate of the curcumin in the gas phase optimized at def2-TZVP level of theory

O	14.5117	-6.7691	16.0957
O	20.4987	-6.8693	28.2342
O	15.7944	-8.9503	15.3302
O	19.3112	-4.6659	29.1076
O	18.3812	-2.2935	20.5274
O	21.0747	-5.7176	20.9155
C	17.8078	-6.1900	17.7049
C	20.1320	-4.9955	25.0412
C	20.3892	-3.5407	20.1988
H	20.8293	-2.6088	20.5558
H	20.8837	-3.8494	19.2796
C	16.4706	-5.9625	17.3217
H	15.9673	-5.0634	17.6452
C	20.4781	-6.0331	25.9287
H	20.9616	-6.9160	25.5335
C	15.8034	-6.8770	16.5336
C	20.2089	-5.9300	27.2810
C	18.4350	-7.3600	17.2656
H	19.4610	-7.5502	17.5553
C	19.5054	-3.8566	25.5628
H	19.2215	-3.0457	24.9060
C	18.5578	-5.2635	18.5379
H	19.5838	-5.5629	18.7249
C	20.4412	-5.1645	23.6322
H	20.8962	-6.1125	23.3567
C	16.4525	-8.0535	16.1029
C	19.5803	-4.7777	27.7844
C	18.9021	-3.2475	19.9717
C	20.6134	-4.6378	21.2432
C	17.7663	-8.2846	16.4738
H	18.2508	-9.1912	16.1360
C	19.2332	-3.7501	26.9168
H	18.7475	-2.8728	27.3237
C	18.1124	-4.1254	19.1037
H	17.0884	-3.7908	18.9807
C	20.2382	-4.2962	22.6251
H	19.7949	-3.3212	22.7849
C	13.7576	-5.6251	16.4727
H	12.7751	-5.7499	16.0238
H	14.2176	-4.7084	16.0937
H	13.6566	-5.5615	17.5596
C	21.1405	-8.0712	27.8315
H	21.2731	-8.6603	28.7359
H	22.1172	-7.8654	27.3846
H	20.5237	-8.6284	27.1210
H	14.8986	-8.6158	15.1794
H	19.6223	-5.4710	29.5460

Table S-VII. Coordinate of the curcumin lifted from the active site of transmembrane serine protease 2 (TMPRSS2) PDB ID: 1Z8A

O	17.5840	-6.0610	14.7080
O	23.1110	-6.7400	26.5750
O	15.7480	-8.1100	14.3190
O	23.0290	-4.5390	28.2700
O	15.2930	-2.7810	21.1560
O	16.3560	-5.2890	23.0120
C	15.9100	-6.1260	17.9410
C	20.1520	-5.0140	25.3410
C	17.4680	-3.7490	21.5280
H	18.0140	-2.7930	21.7060
H	18.2130	-4.2860	20.8960
C	16.7810	-5.7550	16.9280
H	17.5070	-4.9400	17.0880
C	21.1520	-5.9640	25.4640
H	21.1790	-6.8350	24.7880
C	16.7290	-6.4230	15.7050
C	22.1250	-5.8080	26.4520
C	14.9890	-7.1450	17.7620
H	14.3030	-7.4260	18.5790
C	20.0970	-3.9110	26.1790
H	19.2930	-3.1650	26.0660
C	15.9640	-5.4210	19.2340
H	15.8380	-6.0210	20.1510
C	19.1240	-5.1780	24.2990
H	19.0380	-6.1660	23.8160
C	15.8070	-7.4510	15.5100
C	22.0840	-4.7040	27.3030
C	16.2050	-3.4860	20.7330
C	17.2700	-4.4870	22.8380
C	14.9370	-7.8130	16.5380
H	14.2080	-8.6270	16.3840
C	21.0700	-3.7550	27.1670
H	21.0380	-2.8820	27.8400
C	16.1550	-4.1020	19.3730
H	16.2760	-3.4680	18.4790
C	18.2860	-4.2130	23.8960
H	18.3480	-3.2090	24.3490
C	18.8180	-6.7710	14.6200
H	19.5180	-6.4750	13.8040
H	18.6130	-7.8650	14.5540
H	19.3470	-6.7180	15.6000
C	22.9350	-7.7430	27.5740
H	23.7420	-8.5060	27.6750
H	21.9570	-8.2550	27.4180
H	22.7580	-7.2570	28.5620
H	16.3880	-7.7030	13.7110
H	23.6110	-5.3180	28.2800

Table S-VIII. Coordinate of the curcumin lifted from the active site of angiotensin-converting enzyme 2 (ACE2) PDB ID: 3D0G.

O	42.8250	-16.3020	95.6150
O	50.0770	-15.7900	95.8640
O	40.8640	-16.5800	93.6670
O	48.2690	-17.2730	94.3620
O	44.9740	-9.1740	93.7350
O	47.6670	-8.9640	96.8100
C	43.1640	-13.1510	93.8230
C	47.2450	-13.5070	95.7220
C	45.4010	-9.3750	96.0980
H	44.8310	-9.8140	96.9500
H	45.2330	-8.2890	96.2880
C	43.3860	-14.1540	94.7530
H	44.1660	-14.0370	95.5240
C	48.4970	-14.0160	96.0240
H	49.2100	-13.4230	96.6200
C	42.6110	-15.3130	94.7030
C	48.8470	-15.2860	95.5670
C	42.1910	-13.2740	92.8450
H	42.0300	-12.4650	92.1130
C	46.3320	-14.2340	94.9740
H	45.3390	-13.8120	94.7430
C	43.9830	-11.9260	93.8750
H	44.7220	-11.7690	93.0710
C	46.8750	-12.1650	96.2040
H	46.1990	-12.1010	97.0740
C	41.6270	-15.4530	93.7240
C	47.9400	-16.0300	94.8130
C	44.7630	-9.7780	94.7830
C	46.8750	-9.7050	96.2330
C	41.4160	-14.4340	92.7960
H	40.6370	-14.5440	92.0230
C	46.6820	-15.5040	94.5160
H	45.9650	-16.0920	93.9190
C	43.8930	-10.9900	94.8300
H	43.1720	-11.1160	95.6550
C	47.3010	-11.0160	95.6610
H	47.9710	-11.0400	94.7850
C	43.7440	-17.3310	95.2530
H	43.9190	-18.1410	95.9990
H	44.7190	-16.8740	94.9650
H	43.4330	-17.7820	94.2820
C	50.8690	-15.0590	96.7990
H	51.8760	-15.4720	97.0420
H	50.2910	-14.9110	97.7410
H	50.9730	-14.0040	96.4530
H	41.1590	-17.1860	94.3670
H	49.0740	-17.2110	93.8210

Table S-IX. Coordinate of the curcumin lifted from the active site of 3-chymotrypsin-like protease (3CLpro) PDB ID: 3AW0

O	-28.1110	-35.0320	5.3490
O	-18.9650	-41.3030	2.1840
O	-26.3900	-32.8820	5.7220
O	-19.2640	-43.4760	0.4770
O	-24.5710	-40.5870	8.9140
O	-25.7900	-40.3060	4.7770
C	-25.2220	-36.6910	6.8200
C	-22.5060	-42.0400	2.5990
C	-25.2360	-41.5120	6.7900
H	-24.5480	-42.3530	7.0400
H	-26.2200	-42.0250	6.8970
C	-26.4790	-36.5040	6.2660
H	-27.1580	-37.3610	6.1210
C	-21.2750	-41.4240	2.7510
H	-21.1630	-40.5620	3.4300
C	-26.8760	-35.2200	5.8940
C	-20.1780	-41.9050	2.0360
C	-24.3530	-35.6300	7.0120
H	-23.3570	-35.7990	7.4540
C	-22.6720	-43.1240	1.7520
H	-23.6600	-43.6020	1.6440
C	-24.8010	-38.0480	7.2130
H	-23.7220	-38.2310	7.3500
C	-23.6650	-41.5320	3.3540
H	-24.4750	-41.0460	2.7840
C	-26.0120	-34.1410	6.0810
C	-20.3280	-42.9950	1.1790
C	-25.1080	-40.4100	7.8240
C	-25.0280	-41.0800	5.3520
C	-24.7510	-34.3450	6.6400
H	-24.0680	-33.4910	6.7880
C	-21.5750	-43.6040	1.0370
H	-21.6930	-44.4660	0.3590
C	-25.6380	-39.0750	7.4160
H	-26.7240	-38.9330	7.2810
C	-23.8060	-41.6180	4.6840
H	-23.0140	-42.0900	5.2890
C	-28.3040	-35.4820	4.0100
H	-29.3140	-35.3280	3.5640
H	-28.0250	-36.5590	3.9360
H	-27.5320	-35.0230	3.3490
C	-18.6590	-40.2320	1.2930
H	-17.6660	-39.7390	1.4140
H	-19.4640	-39.4630	1.3460
H	-18.7750	-40.5800	0.2400
H	-27.3610	-32.8560	5.6720
H	-18.4710	-42.9660	0.7150

Table S-X. Coordinate of the curcumin lifted from the active site of papain-like protease (PLpro) PDB ID: 3E9S

O	-1.0210	30.1960	14.9090
O	-4.1630	32.2480	14.0690
O	1.2650	29.3220	16.2260
O	-4.0660	32.8400	11.3550
O	-5.8730	24.7800	16.2730
O	-8.5190	25.6350	13.7490
C	-2.0800	26.9030	16.0450
C	-5.2980	29.1040	12.6250
C	-6.1760	25.0910	13.9020
H	-5.4210	25.1480	13.0830
H	-6.4780	24.0210	13.8170
C	-2.1170	28.1500	15.4420
H	-3.0280	28.4910	14.9210
C	-4.9360	30.0520	13.5680
H	-4.9750	29.8110	14.6440
C	-0.9890	28.9690	15.5010
C	-4.5210	31.3150	13.1440
C	-0.9490	26.4530	16.7040
H	-0.9390	25.4570	17.1780
C	-5.2550	29.3840	11.2680
H	-5.5460	28.6160	10.5310
C	-3.2710	26.0360	15.9830
H	-3.2750	25.1250	16.6050
C	-5.7370	27.7720	13.0720
H	-4.9620	27.0620	13.4050
C	0.1580	28.5300	16.1610
C	-4.4720	31.6110	11.7820
C	-5.5100	25.3390	15.2420
C	-7.3550	25.9900	13.5860
C	0.1790	27.2730	16.7630
H	1.0860	26.9270	17.2860
C	-4.8400	30.6470	10.8440
H	-4.8030	30.8830	9.7670
C	-4.3490	26.2770	15.2240
H	-4.3780	27.1740	14.5820
C	-7.0130	27.3610	13.1030
H	-7.8150	28.0400	12.7690
C	-1.4140	31.2990	15.7230
H	-1.4400	32.3030	15.2390
H	-0.7670	31.3410	16.6300
H	-2.4050	31.0840	16.1860
C	-4.4920	31.9720	15.4300
H	-4.1990	32.7360	16.1870
H	-4.0720	30.9810	15.7200
H	-5.5850	31.7660	15.5140
H	1.0130	30.2220	15.9550
H	-3.8470	33.3870	12.1280

Table S-XI. Geometrical parameters of curcumin in the gas phase and the same lifted from the active sites of TMPRSS2 (IIa), ACE2 (IIb), 3CLpro (IIc) and PLpro (IId).

Group		I	IIa	IIb	IIc	IId
Aromatic ring 1				Bond distance, Å		
	C7-C18	1.39830	1.3852	1.3850	1.3848	1.3842
	C18-C30	1.38888	1.3954	1.3959	1.3957	1.3958
	C30-C26	1.38457	1.3945	1.3943	1.3944	1.3939
	C26-C16	1.41102	1.3946	1.3951	1.3949	1.3942
	C16-C12	1.37934	1.3945	1.3951	1.3945	1.3952
	C12-C7	1.40950	1.3865	1.3857	1.3863	1.3856
Aromatic ring 2				Bond distance, Å		
	C8-C20	1.40064	1.3863	1.3862	1.3856	1.3863
	C20-C32	1.38519	1.3954	1.3947	1.3946	1.3954
	C32-C27	1.38895	1.3955	1.3955	1.395	1.3945
	C27-C17	1.40583	1.3945	1.3945	1.3947	1.3947
	C17-C14	1.38268	1.3954	1.3944	1.395	1.3954
	C14-C8	1.40856	1.3848	1.3848	1.3849	1.3853
Aromatic ring 1				Bond angles, °		
	C7-C18-C30	121.3	119.4	119.3	119.3	119.3
	C18-C30-C26	119.9	119.9	120.0	120.0	120.0
	C30-C26-C16	119.6	120.1	120.0	120.1	120.1
	C26-C16-C12	120.3	120.0	120.0	120.0	120.0
	C16-C12-C7	120.5	119.3	119.2	119.3	119.2
	C12-C7-C18	118.4	121.3	121.5	121.4	121.4
Aromatic ring 2	Angles			Bond angles, °		
	C8-C20-C32	121.0	119.3	119.3	119.2	119.3
	C20-C32-C27	120.3	120.0	120.0	120.1	120.0
	C32-C27-C17	119.6	120.0	120.0	120.0	120.1
	C27-C17-C14	119.9	120.0	120.0	120.0	120.0
	C17-C14-C8	120.9	119.3	119.4	119.3	119.4
	C14-C8-C20	118.3	121.4	121.4	121.4	121.3
Chain				Dihedral angles, °		
	C7-C22-C34-C28	178.0	-179.5	-179.5	-179.5	-179.5
	C22-C34-C28-C9	5.2	73.8	-135.7	-111.7	-141.1
	C34-C28-C9-C29	-80.3	-119.1	104.3	36.9	-93.1
	C28-C9-C29-C36	-67.5	-152.4	-39.1	112.5	79.3
	C9-C29-C36-C24	-177.3	-113.4	-66.7	166.2	-5.4
	C29-C36-C24-C8	-179.9	-179.5	-179.5	-179.5	-179.5
Chain				Bond distance, Å		
	C8-C24	1.45239	1.47290	1.47316	1.47356	1.47199
	C24-C36	1.34514	1.34010	1.34035	1.34022	1.34092
	C36-C29	1.47211	1.49221	1.49244	1.49297	1.49328
	C29-C9	1.53123	1.51656	1.51651	1.51583	1.51595
	C9-C28	1.53265	1.51538	1.51614	1.51656	1.51679
	C28-C34	1.46552	1.49384	1.49267	1.49318	1.49268
	C34-C22	1.34677	1.33999	1.34023	1.34034	1.34024
	C22-C7	1.45423	1.47370	1.47448	1.47416	1.47445
	C29-O6	1.21908	1.22836	1.22853	1.22896	1.22780
	C28-O5	1.22076	1.22788	1.22786	1.22792	1.22769
	C27-O4	1.35491	1.36211	1.36260	1.36245	1.36294
	C17-O2	1.36925	1.36233	1.36260	1.36223	1.36172
	C26-O3	1.35440	1.36244	1.36218	1.36266	1.36270
	C16-O1	1.36817	1.36238	1.36223	1.36294	1.36272

Table S-XII. Detailed summary of Mulliken population analysis (MPA) and natural population analysis (NPA) charges of curcumin in gas phase (I) and curcumin lifted from the active site of (b) transmembrane serine protease 2 (TMPRSS2) PDB ID: 1Z8A (IIa), (c) angiotensin-converting enzyme 2 (ACE2) PDB ID: 3D0G (IIb), (d) 3-chymotrypsin-like protease (3CLpro) PDB ID: 3AW0 (IIc) and (e) papain-like protease (PLpro) PDB ID: 3E9S (IId). The calculation is performed at B3LYP/def2-TZVP level of theory.

Curcumin		I	I	IIa	IIa	IIb	IIb	IIc	IIc	IId	IId
Sequence Number	Atom Symbol	MPA, e	NPA, e	MPA, e	NPA, e	MPA, e	NPA, e	MPA, e	NPA, e	MPA, e	NPA, e
1	O	-0.34563	-0.48409	-0.35051	-0.50581	-0.34798	-0.50634	-0.35644	-0.50833	-0.33756	-0.50172
2	O	-0.34552	-0.48398	-0.34018	-0.50261	-0.2836	-0.45772	-0.35045	-0.50514	-0.34102	-0.48199
3	O	-0.38681	-0.63191	-0.39929	-0.64285	-0.39646	-0.64221	-0.40884	-0.64768	-0.38819	-0.63608
4	O	-0.38775	-0.63212	-0.38995	-0.64007	-0.42946	-0.66471	-0.39773	-0.6432	-0.39995	-0.64037
5	O	-0.31345	-0.54325	-0.28097	-0.49423	-0.29018	-0.51148	-0.27884	-0.50347	-0.28818	-0.50889
6	O	-0.33479	-0.559	-0.30249	-0.51179	-0.27549	-0.49379	-0.33061	-0.53663	-0.283	-0.49625
7	C	0.13326	-0.1051	0.24018	-0.10286	0.22315	-0.11405	0.23682	-0.10156	0.24939	-0.11455
8	C	0.23511	-0.10494	0.26268	-0.10899	0.06402	-0.08182	0.19978	-0.113	0.09404	-0.10695
9	C	-0.14137	-0.57914	-0.23387	-0.59987	-0.20352	-0.60048	-0.21577	-0.59736	-0.14111	-0.59554
10	H	0.1165	0.24062	0.13782	0.24843	0.12723	0.23957	0.12073	0.23431	0.13364	0.225
11	H	0.12212	0.22952	0.13569	0.24653	0.1383	0.25891	0.13711	0.26319	0.12805	0.25944
12	C	-0.33067	-0.24997	-0.28759	-0.20999	-0.28569	-0.23003	-0.25196	-0.20657	-0.19996	-0.19958
13	H	0.12873	0.21338	0.11896	0.21897	0.15095	0.23174	0.1225	0.21922	0.10724	0.21413
14	C	-0.3196	-0.24068	-0.30899	-0.19752	-0.29467	-0.26476	-0.28309	-0.21102	-0.33625	-0.26737
15	H	0.13047	0.21368	0.11406	0.21986	0.11399	0.22101	0.12789	0.22514	0.1555	0.21427
16	C	0.34123	0.22379	0.26257	0.20379	0.22971	0.20741	0.24608	0.21316	0.20376	0.21147
17	C	0.32459	0.21373	0.26533	0.2041	0.29276	0.24351	0.27688	0.20609	0.35394	0.22617
18	C	-0.17153	-0.16122	-0.19352	-0.17354	-0.19417	-0.17784	-0.20341	-0.17568	-0.17304	-0.16262
19	H	0.11884	0.21364	0.11744	0.21723	0.11913	0.21952	0.10688	0.2125	0.11549	0.21723
20	C	-0.18438	-0.16599	-0.14899	-0.16894	-0.15615	-0.21804	-0.16854	-0.18008	-0.1893	-0.19542
21	H	0.11428	0.21231	0.10164	0.20996	0.24189	0.22004	0.11612	0.21656	0.11467	0.21891
22	C	-0.06459	-0.1032	-0.18668	-0.15483	-0.16767	-0.10785	-0.17416	-0.14112	-0.20351	-0.0909
23	H	0.13719	0.21665	0.13677	0.21552	0.13531	0.2197	0.10102	0.20383	0.12365	0.21794
24	C	-0.11913	-0.07977	-0.16874	-0.13451	-0.22839	-0.14582	-0.12144	-0.06783	-0.08674	-0.11201
25	H	0.11747	0.21388	0.11177	0.20656	0.12025	0.19909	0.14488	0.22229	0.12859	0.19898
26	C	0.18269	0.27931	0.1669	0.24971	0.15455	0.25076	0.16694	0.25042	0.17703	0.25822
27	C	0.17419	0.27689	0.16268	0.25325	0.21694	0.22745	0.15689	0.2507	0.16409	0.24794
28	C	0.15692	0.52655	0.25821	0.56067	0.273	0.5418	0.14805	0.55414	0.19004	0.53778
29	C	0.20286	0.53703	0.20127	0.55782	0.18926	0.55985	0.30592	0.53452	0.19593	0.52913
30	C	-0.20365	-0.25309	-0.20859	-0.23992	-0.19409	-0.23775	-0.19799	-0.24143	-0.21829	-0.24124
31	H	0.11323	0.22326	0.11442	0.22325	0.11736	0.22427	0.11248	0.222	0.11899	0.22579
32	C	-0.18847	-0.24377	-0.22177	-0.23601	-0.25726	-0.22518	-0.19986	-0.23754	-0.19101	-0.23078
33	H	0.11533	0.22317	0.11721	0.22387	0.11222	0.21626	0.11599	0.22396	0.11858	0.22702
34	C	-0.14545	-0.30723	-0.14817	-0.29466	-0.17835	-0.3	-0.03469	-0.28283	-0.14413	-0.32849
35	H	0.08325	0.20485	0.12793	0.22155	0.1276	0.21434	0.1064	0.2181	0.09229	0.19591
36	C	-0.23364	-0.32978	-0.10318	-0.29563	-0.11374	-0.2844	-0.23287	-0.31913	-0.17246	-0.28048
37	H	0.13062	0.21134	0.11573	0.2124	0.13883	0.23168	0.12708	0.21135	0.12622	0.22473
38	C	-0.20067	-0.24674	-0.18784	-0.25576	-0.15926	-0.25625	-0.1702	-0.25155	-0.16392	-0.25306
39	H	0.13627	0.19673	0.13876	0.20143	0.13864	0.20353	0.13291	0.19903	0.1404	0.20649
40	H	0.12737	0.17574	0.11664	0.16248	0.07241	0.17893	0.12261	0.17241	0.11142	0.15256
41	H	0.12904	0.17617	0.11514	0.17056	0.11663	0.1567	0.11249	0.16767	0.08497	0.16837
42	C	-0.20035	-0.24622	-0.19482	-0.25703	-0.19847	-0.25598	-0.19225	-0.25542	-0.23597	-0.25451
43	H	0.13558	0.19621	0.14146	0.20359	0.14336	0.20698	0.14039	0.20256	0.15155	0.20683
44	H	0.12839	0.17516	0.12184	0.17401	0.12611	0.17248	0.12153	0.17156	0.12053	0.16569
45	H	0.12841	0.1752	0.10756	0.15653	0.12195	0.16789	0.1168	0.16266	0.14804	0.18028
46	H	0.3268	0.49129	0.32349	0.48239	0.3237	0.48365	0.32285	0.4853	0.32344	0.48294
47	H	0.32671	0.49106	0.32198	0.48298	0.32533	0.47945	0.32314	0.4839	0.32212	0.48556

Table S XIII. Detailed summary of electron density, ρ_{bcp} (r) and Laplacian of electron density, $\nabla^2\rho_{bcp}$(r) of curcumin in gas phase (I) and curcumin lifted from the active site of (b) transmembrane serine protease 2 (TMPRSS2) PDB ID: 1Z8A (IIa), (c) angiotensin-converting enzyme 2 (ACE2) PDB ID: 3D0G (IIb), (d) 3-chymotrypsin-like protease (3CLpro) PDB ID: 3AW0 (IIc) and (e) papain-like protease (PLpro) PDB ID: 3E9S (IId). The calculation is performed at B3-LYP/def2-TZVP level of theory

Curcumin	I		IIa		IIb		IIc		IId	
Bond	ρ_{bcp} (r), a.u.	$\nabla^2\rho_{bcp}$(r), a.u.	ρ_{bcp} (r), a.u.	$\nabla^2\rho_{bcp}$(r), a.u.	ρ_{bcp} (r), a.u.	$\nabla^2\rho_{bcp}$(r), a.u.	ρ_{bcp} (r), a.u.	$\nabla^2\rho_{bcp}$(r), a.u.	ρ_{bcp} (r), a.u.	$\nabla^2\rho_{bcp}$(r), a.u.
O1-C38	0.2511	-0.5045	0.2519	-0.5639	0.2509	-0.5516	0.2509	-0.5504	0.2519	-0.5608
O2-C17	0.2872	-0.5830	0.2914	-0.5827	0.2915	-0.5761	0.2915	-0.5833	0.2897	-0.5296
O2-C42	0.2515	-0.5078	0.2521	-0.5655	0.2510	-0.5435	0.2515	-0.5601	0.2497	-0.5301
O3-C26	0.3003	-0.6409	0.2947	-0.6446	0.2952	-0.6502	0.2950	-0.6562	0.2952	-0.6576
O3-H46	0.3555	-2.4420	0.3523	-2.3750	0.3525	-2.3810	0.3510	-2.3690	0.3514	-2.3630
O4-H47	0.3555	-2.4410	0.3520	-2.3710	0.3507	-2.3370	0.3516	-2.3720	0.3521	-2.3810
O6-C29	0.4150	-0.2481	0.4075	-0.3306	0.4076	-0.3334	0.4068	-0.3333	0.4087	-0.3393
C7-C12	0.3076	-0.8863	0.3220	-0.9593	0.3211	-0.9469	0.3227	-0.9647	0.3235	-0.9724
C7-C18	0.3169	-0.9326	0.3243	-0.9754	0.3227	-0.9619	0.3248	-0.9793	0.3257	-0.9864
C7-C22	0.2854	-0.8065	0.2755	-0.7637	0.2761	-0.7736	0.2749	-0.7571	0.2750	-0.7554
C8-C14	0.3090	-0.8925	0.3241	-0.9733	0.3223	-0.9571	0.3220	-0.9558	0.3212	-0.9497
C8-C20	0.3147	-0.9232	0.3239	-0.9745	0.3217	-0.9530	0.3226	-0.9628	0.3214	-0.9514
C8-C24	0.2865	-0.8135	0.2756	-0.7598	0.2769	-0.7812	0.2771	-0.7794	0.2775	-0.7815
C9-C28	0.2481	-0.6202	0.2597	-0.6867	0.2589	-0.6802	0.2556	-0.6600	0.2560	-0.6624
C9-C29	0.2497	-0.6283	0.2568	-0.6674	0.2562	-0.6641	0.2591	-0.6804	0.2559	-0.6619
C9-H10	0.2804	-0.9676	0.2637	-0.8617	0.2631	-0.8554	0.2676	-0.8849	0.2659	-0.8670
C9-H11	0.2829	-0.9839	0.2648	-0.8686	0.2658	-0.8792	0.2613	-0.8491	0.2669	-0.8860
C12-H13	0.2882	-1.0260	0.2743	-0.9451	0.2787	-0.9638	0.2750	-0.9485	0.2749	-0.9459
C14-C17	0.3249	-0.9672	0.3201	-0.9461	0.3204	-0.9498	0.3203	-0.9482	0.3189	-0.9362
C14-H15	0.2872	-1.0210	0.2744	-0.9471	0.2762	-0.9490	0.2748	-0.9497	0.2749	-0.9381
C16-C12	0.3266	-0.9719	0.3205	-0.9471	0.3198	-0.9438	0.3206	-0.9449	0.3198	-0.9400
C16-C26	0.3168	-0.9510	0.3246	-0.9791	0.3243	-0.9758	0.3246	-0.9816	0.3253	-0.9875
C16-O1	0.2879	-0.5817	0.2909	-0.5741	0.2918	-0.5893	0.2913	-0.5904	0.2917	-0.5967
C17-C27	0.3194	-0.9619	0.3247	-0.9787	0.3244	-0.9857	0.3246	-0.9779	0.3238	-0.9810
C18-C30	0.3201	-0.9487	0.3161	-0.9223	0.3155	-0.9191	0.3160	-0.9220	0.3161	-0.9233
C18-H19	0.2879	-1.0310	0.2754	-0.9532	0.2757	-0.9553	0.2752	-0.9509	0.2756	-0.9547
C20-C32	0.3220	-0.9551	0.3158	-0.9179	0.3158	-0.9224	0.3163	-0.9236	0.3159	-0.9242
C20-H21	0.2889	-1.0370	0.2761	-0.9544	0.2800	-0.9646	0.2755	-0.9533	0.2750	-0.9497
C22-C34	0.3463	-1.0660	0.3472	-1.0420	0.3489	-1.0600	0.3474	-1.0470	0.3501	-1.0770
C22-H23	0.2899	-1.0460	0.2762	-0.9562	0.2764	-0.9596	0.2758	-0.9524	0.2776	-0.9694
C24-C25	0.2883	-1.0360	0.2762	-0.9565	0.2742	-0.9388	0.2772	-0.9677	0.2818	-0.9713
C24-C36	0.3473	-1.0710	0.3482	-1.0560	0.3467	-1.0350	0.3507	-1.0810	0.3498	-1.0700
C26-C30	0.3267	-0.9919	0.3203	-0.9586	0.3206	-0.9601	0.3205	-0.9583	0.3209	-0.9619
C27-C32	0.3242	-0.9815	0.3200	-0.9594	0.3196	-0.9440	0.3201	-0.9576	0.3197	-0.9510
C27-O4	0.3000	-0.6394	0.2948	-0.6432	0.2953	-0.6663	0.2948	-0.6489	0.2948	-0.6559
C28-O5	0.4143	-0.2675	0.4078	-0.3170	0.4078	-0.3187	0.4077	-0.3235	0.4082	-0.3262
C29-C36	0.2806	-0.7786	0.2721	-0.7501	0.2731	-0.7611	0.2706	-0.7328	0.2708	-0.7366

Curcumin	I		IIa		IIb		IIc		IId	
Bond	ρ_{bcp} (r), a.u.	$\nabla^2\rho_{bcp}$(r), a.u.	ρ_{bcp} (r), a.u.	$\nabla^2\rho_{bcp}$(r), a.u.	ρ_{bcp} (r), a.u.	$\nabla^2\rho_{bcp}$(r), a.u.	ρ_{bcp} (r), a.u.	$\nabla^2\rho_{bcp}$(r), a.u.	ρ_{bcp} (r), a.u.	$\nabla^2\rho_{bcp}$(r), a.u.
C30-H31	0.2870	-1.0260	0.2742	-0.9451	0.2746	-0.9477	0.2741	-0.9441	0.2749	-0.9502
C32-H33	0.2872	-1.0280	0.2748	-0.9495	0.2751	-0.9472	0.2745	-0.9475	0.2745	-0.9483
C34-C28	0.2841	-0.7991	0.2723	-0.7556	0.2722	-0.7478	0.2717	-0.7469	0.2703	-0.7293
C34-H35	0.2859	-1.0120	0.2720	-0.9279	0.2733	-0.9361	0.2722	-0.9279	0.2772	-0.9367
C36-H37	0.2871	-1.0200	0.2721	-0.9254	0.2729	-0.9386	0.2748	-0.9445	0.2756	-0.9575
C38-H39	0.2899	-1.0470	0.2714	-0.9331	0.2714	-0.9326	0.2715	-0.9334	0.2719	-0.9362
C38-H40	0.2853	-1.0100	0.2721	-0.9180	0.2745	-0.9301	0.2728	-0.9238	0.2714	-0.9115
C38-H41	0.2853	-1.0100	0.2724	-0.9217	0.2717	-0.9135	0.2722	-0.9195	0.2745	-0.9279
C42-H43	0.2898	-1.0460	0.2715	-0.9338	0.2715	-0.9343	0.2714	-0.9332	0.2718	-0.9352
C42-H44	0.2851	-1.0090	0.2726	-0.9228	0.2723	-0.9195	0.2727	-0.9231	0.2745	-0.9259
C42-H45	0.2852	-1.0090	0.2718	-0.9148	0.2729	-0.9206	0.2721	-0.9179	0.2725	-0.9213

Table S-XIV. HUMO-LUMO band gap and dipole moments of curcumin in the gas phase and that lifted from the active site of TMPRSS2 (IIa), ACE2 (IIb), 3CLpro (IIc) and PLpro (IId)

Structure	I	IIa	IIb	IIc	IId
HOMO-LUMO band gap, eV	3.699	4.367	4.392	3.714	4.058
μ_x , D	-0.632	2.574	0.317	0.328	1.725
μ_y , D	-1.058	-1.003	-1.547	-0.036	2.033
μ_z, D	0.355	-0.044	0.412	-1.711	0.218
μ, D	3.26	7.022	4.147	4.429	6.8

μ_x, μ_y and μ_z are the dipole moments in *x*, *y*, and *z*-directions whereas μ represents the resultant dipole moment